Strategy to Design a Flexible and Macromolecular Sensor to Bind Cd²⁺ Ions: A Complete Photophysical Analysis and Bio-Imaging Study

Surajit Mondal and Swapan Dey*
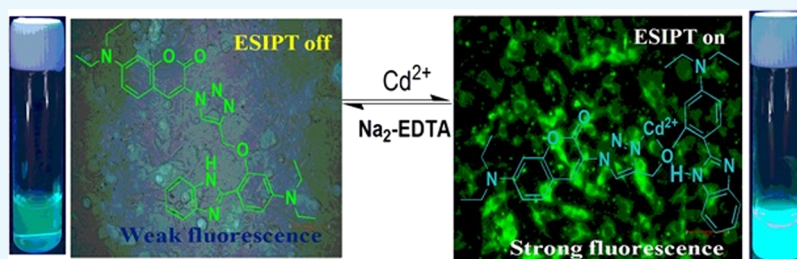
Read Online

ACCESS | Metrics & More | Article Recommendations | Supporting Information

ABSTRACT: A novel triazole-bridged coumarin−benzimidazole-conjugated fluorescence sensor (**4**) has been developed for selective detection of Cd²⁺ over other competitive metal ions. The sensor exhibited quick "turn-on" responses upon interaction with a very low level of Cd²⁺ (14 nM). The photophysical changes in the complexation of Cd²⁺ with sensor **4** have been explained through the excited-state intramolecular proton transfer mechanism. The involvement of benzimidazole and triazole moieties in Cd²⁺ binding was confirmed by different spectroscopic techniques such as UV−vis, Fourier transform infrared, nuclear magnetic resonance, and ESI mass. The diameter of the circular shape of the sensor decreased upon complexation with Cd²⁺, which was confirmed by field-emission scanning electron microscopy. Furthermore, the quantum chemical (density functional theory) calculation supported the mechanism of interactions and the mode of binding of **4** toward Cd²⁺. The sensor was more effective for finding Cd²⁺ in two living cells, C6 (rat glial cell) and Hep G2 (human liver cell).

1. INTRODUCTION

Increasing cadmium contamination in the environment through industrial waste has created serious problems for human health. Cadmium has been extensively used in many industrial processes such as electroplating, war industry, coloring matters, and the preparation of phosphate fertilizers.[1,2] The exposure of cadmium in the environment, particularly in water and soil, has occurred and led to bioaccumulation through the food chain.[3−6] The excessive level of Cd²⁺ created many fatal problems like heart disease, cardiovascular diseases, diabetes, and even may initiate cancer.[7−10] Thus, selective and sensitive methodologies are highly needed for low-level detection of Cd²⁺ without any interference.

Several processes, such as atomic absorption spectroscopy and inductively coupled plasma−mass spectrometry based on advanced technology, have been extensively used for the detection of Cd²⁺.[11−15] In this regard, the fluorescent technique is superior compared to others for its simplicity, selectivity, and low cost.[16−20] A fluorophore may change its output signal through different mechanistic aspects upon binding with the particular analyte.[21] Among various mechanisms associated with the fluorescent sensor, the excited-state intramolecular proton transfer (ESIPT) has

several significant advantages over others.[22,23] The ESIPT-based probes consist of a unique framework having intramolecular hydrogen bonding between a hydrogen bond donor (−OH and −NH₂) and hydrogen bond acceptor (C═N and C═O). The large Stokes shift was often found in ESIPT-based fluorophores compare to others.[24,25]

In this context, the benzimidazole moiety has been utilized to develop ESIPT-based probes for toxic metal ions. The derivatives of benzimidazole are widely used as antifungal and anthelmintic drugs for a long time.[26] Like imidazole, coumarin derivatives also have some special characters like high quantum yield, readily soluble in a polar protic solvent, and so forth, which attract their searchers to utilize them as fluorophores to develop a chemical sensor for a particular analyte.[27] Keeping these points in mind, we report here a triazole-bridged coumarin−benzimidazole-conjugated turn-on sensor for the
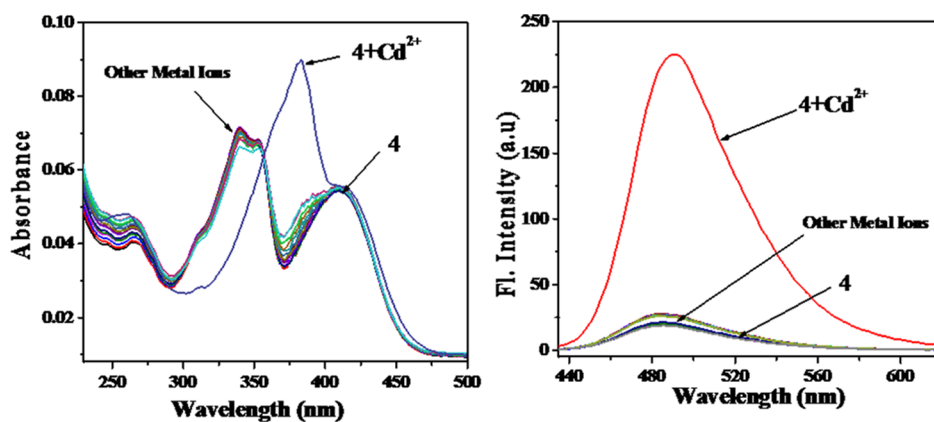
Figure 1. UV−vis (λ_{max} = 382 nm) and emission responses (λ_{ex} = 380 nm) of 4 (8.6 μM) with other metal ions (10 mM) (λ_{em} = 485 nm) in ACN.

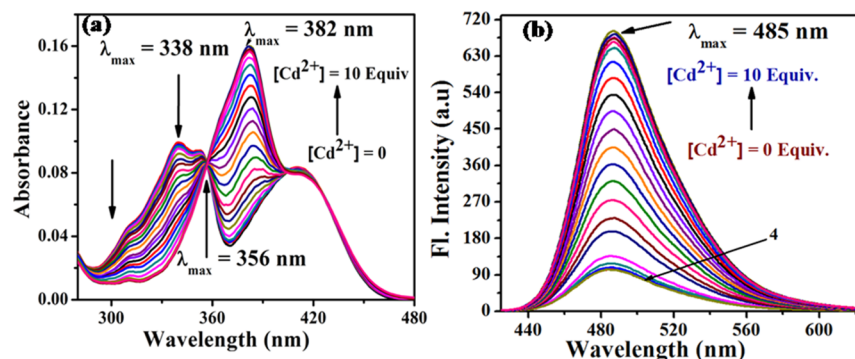**Figure 2.** (a) UV−vis and (b) fluorescence titration experiment of 4 (8.6 μM) with Cd^{2+} (50.03 μM) in ACN, λ_{ex} = 380 nm.

selective detection of Cd^{2+} through the ESIPT mechanism. To the best of our knowledge, a coumarin−triazole-based sensor for selective quantification of Cd^{2+} is very rare to date, and recently reported sensors for Cd^{2+} are given in Supporting Information Table S2. Indeed, the triazole-bridged coumarin−benzimidazole scaffold turn-on sensor for selective detection of Cd^{2+} through the ESIPT mechanism is entirely unknown. Besides, many of the reported sensors suffer not only on selectivity issues but also on problems in the detection limit.[28,29] As a part of our ongoing research on the development of organic sensors for heavy and toxic metal ions,[30−32] we resolve all such problems by designing a novel turn-on sensor (4) toward the detection of Cd^{2+}.

2. RESULTS AND DISCUSSION

2.1. Design and Synthesis. Compound 1 was first synthesized from 4-(diethylamino)salicylaldehyde, and compound 2 has been prepared from the corresponding amine, ensuing a reported procedure.[33] The triazole moiety of compound (3) was developed by the reaction between compound 1 and compound 2 via "click reaction" in the presence of sodium ascorbate. The corresponding azide from the amine was afforded following the reported procedure, as mentioned in the experimental section. Sensor 4 was synthesized from the reaction of compound 3 with o-phenylenediamine in the presence of sodium bisulfite.

2.2. Photophysical Properties of the Sensor. The detailed sensing behavior of the sensor has been investigated by UV−vis and fluorescence experiments at room temperature. Initially, the sensor was non-fluorescent in acetonitrile (ACN) and became highly blue-fluorescent on adding Cd^{2+}, which was

easily noticeable through the naked eye. A series of metal ions like Li^+, Na^+, K^+, Ca^{2+}, Mg^{2+}, Mn^{2+}, Co^{2+}, Ni^{2+}, Cu^{2+}, Ag^+, Cr^{3+}, Zn^{2+}, Fe^{3+}, Cd^{2+}, Ba^{2+}, Hg^{2+}, and Pb^{2+} were applied to explore the photophysical complexation responses of 4 in ACN. Among the series of metal ions, only Cd^{2+} caused significant changes in the fluorescent properties of the sensor and weak fluorescence turned into greenish-blue fluorescence under a long-wavelength UV lamp (Figure S1, Supporting Information). In comparison, other metal ions were not able to produce any detectable color change in the sensor.

The UV−vis and fluorescence spectra were taken in ACN to establish a better conclusion on the selectivity of the sensor (4). The sensor exhibited two absorption maxima at 338 and 410 nm in UV−vis spectroscopy, which were assigned for benzimidazole and coumarin moieties, respectively. A new peak at λ_{max} 382 nm appeared upon the addition of Cd^{2+} and the weak fluorescence turned into strong fluorescence. In a fluorescence experiment, a peak at λ_{em} 485 nm appeared when the sensor itself was excited at λ_{ex} = 380 nm. After the addition of the analyte, the emission intensity dramatically enhanced at λ_{em} 485 nm without any spectral shift. Other metal ions did not induce any significant changes (Figure 1). Both these findings indicated that sensor 4 was highly selective toward Cd^{2+} over other metal ions.

The titration experiment of the sensor with the increasing concentration of Cd^{2+} was carried out in UV−vis and fluorescence techniques to acquire the more fundamental results about complexation. With the increasing concentration of Cd^{2+}, the change in absorption spectra was recorded, and the corresponding results are shown in Figure 2. The absorption intensity at 338 nm was gradually decreased, and

immediately, a new absorption maximum at 382 nm was generated with the appearance of an isosbestic point at 356 nm. The appearance of an isosbestic point upon the addition of Cd^{2+} in the absorption spectra indicated the successful complex formation between the sensor and metal ion.

Surprisingly, no significant changes were observed in the absorption maxima of the sensor at 412 nm, which was mainly originated from the coumarin moiety. Therefore, to carry out emission experiments, 380 nm was used as an excitation wavelength.

Fluorescence titration has been carried out to get a quantitative idea about the complexation in ACN. The free receptor exhibited a very weak emission maximum at 485 nm upon excitation at 380 nm. When Cd^{2+} was added to **4**, the emission intensity of the sensor dramatically enhanced without any spectral shift and the sensor turned on due to the ESIPT process, whereas no such spectral change for **4** was found with other metal ions. These findings suggested selective complexation between **4** and Cd^{2+}. The quantum yield (ϕ) of the sensor increased abruptly after the addition of Cd^{2+}, and the corresponding values were 0.10 and 0.49 for **4** and **4:Cd^{2+}**, respectively, where lucifer yellow CH was used as a standard in water. The high value of quantum yield in the complex may be attributed to the rigidification through coordination, which further restricts the non-radiative decay. The limit of detection was calculated using the fluorescence titration data[34,35] and was found to be 14.0 nM. Although very few sensors have been previously reported in the literature for Cd^{2+}, sensor **4** showed a better detection limit compared to others. The binding efficiency (K_a) toward the metal ion was measured from the fluorescence titration data and calculated by using the Benesi–Hildebrand linear regression analysis[36,37] and was found to be 0.24×10^4 M^{-1}. The high value of the association constant (K_a) implied the higher affinity of the sensor toward Cd^{2+}.

2.3. Interference and pH Study. The interference study of **4** toward Cd^{2+} has been performed in the presence of other metal ions in the fluorescence experiment. The sensor selectively detected Cd^{2+} in the presence of other metal ions, and it did not interfere in the complexation (Figure 3).
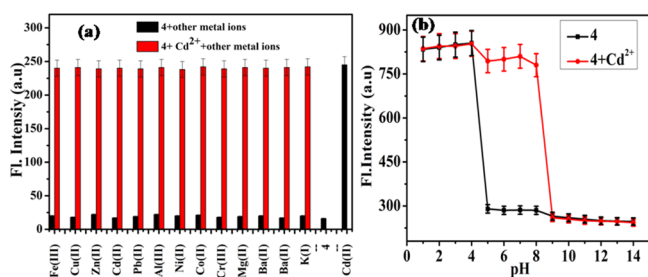

Figure 3. (a) Interference study of sensor **4** (8.6 μM) in the presence of other metal and (b) effect of pH on the emission intensity at λ_{em} 485 nm of **4** and **4:Cd^{2+}** (λ_{ex} 380 nm).

The effect of pH on the photophysical properties of **4** and its complex was examined to get the better usability of the sensor. Figure 3b demonstrates the emission behavior of **4** and **4:Cd^{2+}** at different pH values at 485 nm (λ_{ex} = 380 nm). Initially, the sensor itself exhibited weak fluorescence between pH 5–9. Beyond pH 9.0, the emission intensity suddenly decreased, and this might be due to the deprotonation of benzimidazole −**NH**−, which further disconnected the ESIPT process resulting in turn-off response of the sensor. Whereas the

fluorescent intensity dramatically enhanced at very acidic pH; this might be due to the protonation of the "**O**" atom, which again turned the sensor ESIPT on as depicted in Scheme 2.[38] Upon addition of Cd^{2+} to **4**, the emission intensity increased between pH 5−9 and the sensor did not identify Cd^{2+} at high acidic and basic pH.

The reversibility of a sensor played a significant role in exploring its application in biological sciences. Thus, the reversibility of **4** was also inspected using EDTA as a chelating ligand in ACN, as shown in Figure S14, Supporting Information. The addition of Cd^{2+} enhanced the fluorescent intensity of the sensor immediately at λ_{max} 485 nm upon excitation at 380 nm. Consequently, the fluorescent intensity was quenched upon the addition of EDTA, which quickly encapsulated Cd^{2+} from the sensor. Furthermore, with the addition of Cd^{2+} to this solution, the emission intensity regenerated, and these results implied the reversible complexation nature of the sensor.

2.4. FTIR and NMR Spectra. The Fourier transform infrared (FTIR) spectra of the sensor and its complex had been gathered to get a deep insight into the complexation. The detailed spectral changes upon the addition of Cd^{2+} to **4** are shown in Figure 4a. The triazole C−H and benzimidazole N−H appeared in their respective region 3165 and 3440 cm^{-1}. The peaks were shifted to 3140 and 3290 cm^{-1}, respectively, after complexation. So, the triazole and benzimidazole moieties are both involved in the complexation.

To establish the mode of binding and the mechanism of complexation of the sensor, ^1H NMR titration of the sensor with Cd^{2+} was carried out in CD_3CN at room temperature. Figure 4b demonstrates the ^1H NMR spectra of **4** with different concentrations of Cd^{2+}. Upon addition of Cd^{2+}, the triazole proton, labeled H_a, was shifted continuously upfield from δ 8.31 ppm to δ 8.24 ppm, indicating the participation of the triazole N atom to coordinate Cd^{2+}. The methylene proton, denoted as H_b, moved regularly upfield from δ 5.56 to δ 5.37 ppm with the increase in Cd^{2+}. A new peak appeared at δ 13.36 ppm after the addition of 1.0 equivalent of Cd^{2+}, and this was the evidence of the intramolecular H bonding upon complexation [Figure 5].

2.5. Sensing Mechanism and ESI Mass Analysis. The probable sensing mechanism of sensor **4** for the quantification of Cd^{2+} is explained in Figure 5. The coordination of Cd^{2+} to the sensor could "turn on" the ESIPT process, and the emission intensity was gradually increased. The evidence for the ESIPT might be rationalized based on two successive facts. First, the presence of a singlet at δ 13.36 ppm was found in ^1H NMR of the complex, which was supposed to be due to the intramolecular H bonding between ether **O** and **H−N** of benzimidazole as shown in Figure 5.[39] This intramolecular hydrogen bonding after complex formation might be the driving force for the ESIPT process.[40] Second, a significant Stokes shift implied the characteristics of ESIPT.[41] Excitation of the sensor at 380 nm resulted in an intense emission band at 485 nm with a large Stokes shift of 105 nm. The high value of shift in wavelength further confirmed the ESIPT process.[42]

The photophysical study revealed the binding stoichiometry between the sensor and Cd^{2+} to be 1:1. The result was also confirmed by the ESI mass analysis of the complex. A peak was obtained at 828.08 in ESI mass spectroscopy (Figure S15, Supporting Information), which was assigned to [**4** + Cd + ClO_4 + K−H]. Accordingly, the possible binding mode is depicted in Figure 5, where one Cd^{2+} ion is encapsulated by

Scheme 1. Reagent and Conditions: (i) CuSO₄, 5H₂O, Sodium Ascorbate, EtOH/H₂O(1:1), and 24 h and (ii) o-Phenylenediamine, Sodium Bisulfite, Methanol, Reflux, and 4 h
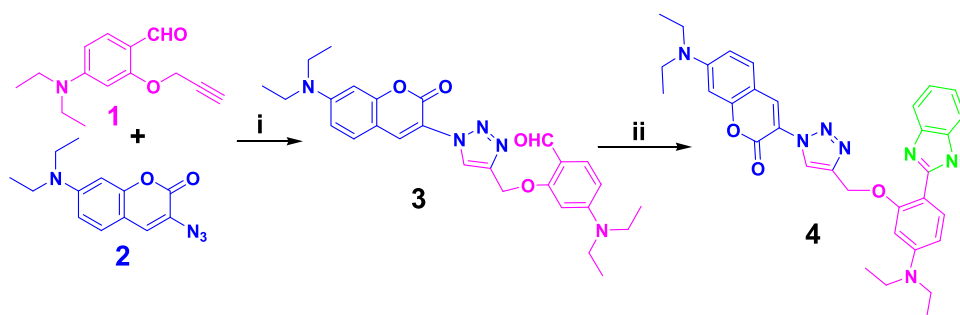
Scheme 2. ESIPT Switching Mechanism of 4 in Acid and Base
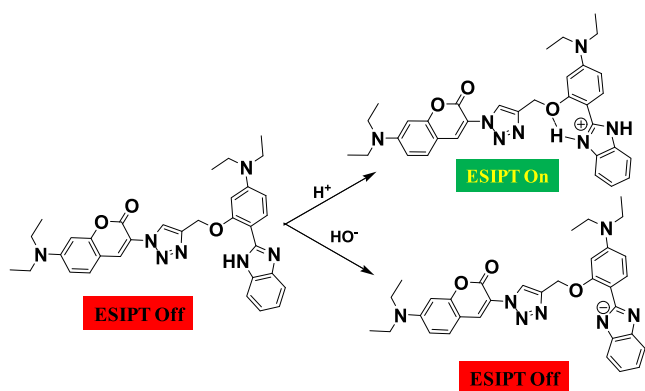
one sensor molecule through common three coordination.[43] Each Cd^{2+} ion was confined with the **O** atom of ether linkage and **N** atoms of triazole (**N3** of 1,2,3-triazole was reported for coordination).[44] Therefore, the small sensor molecule **4** offered a suitable cavity for encapsulating the Cd^{2+} ion tightly.

2.6. Quantum Chemical (Density Functional Theory) Calculation. To support the complexation of **4:Cd²⁺**, the quantum chemical calculation has been carried out using Gaussian 09 software with the aid of the Gauss-View 5.0 visualization program.[45,46] The structures of the sensor and the complex were optimized using the B3LYP/6-311G+ basis set and LanL2MB basis set, respectively. The energy-optimized structures of the sensor and the complex are depicted in Figure 6a. The H atom of the benzimidazole moiety attained the optimum hydrogen bond-forming distance (1.57 Å), which

was attributed to the optimized structure of the complex.[47] Again, the total energy of the complex was lower (−1921.5150 a.u.) than the sensor itself (−1887.39 a.u.), which implied the higher stability of the complex.

Furthermore, the energy of the highest occupied molecular orbital (HOMO) and the lowest unoccupied molecular orbital (LUMO) of the sensor and its complex, along with their spatial distribution, was calculated and is shown in Figure 6b. The HOMO of the sensor was mainly spread over the benzimidazole moiety, whereas the LUMO was on the coumarin moiety. After complexation, the HOMO spread over only the metal ion, but LUMO was located throughout the coumarin moiety. From the energy level diagram, it was easily visualized that the energy gap between the HOMO and the LUMO was decreased after complexation, and this resulted not only in the better stability of complex compared to the sensor itself but also demonstrated a bathochromic shift in UV−vis spectra.[48]

2.7. FESEM Analysis. The field-emission scanning electron microscopy (FESEM) analysis was carried out to get the details about the surface morphological changes of **4** upon complexation. The corresponding FESEM images of **4** and **4:Cd²⁺** are shown in Figure 7a−d. The sensor exhibited a circular shape with a diameter of 2.09 μm in the absence of Cd^{2+} (Figure 7a,b). After the inclusion of Cd^{2+}, the abrupt shrinkage of the area of the circular shape was noticed (diameter was reduced to 1.4 μm as shown in Figure 7d) along with the deformation of the regular shape. The morphological changes upon complexation clearly demonstrated that the complex (**4:Cd²⁺**) has distinct properties compared to the sensor (**4**).[49]
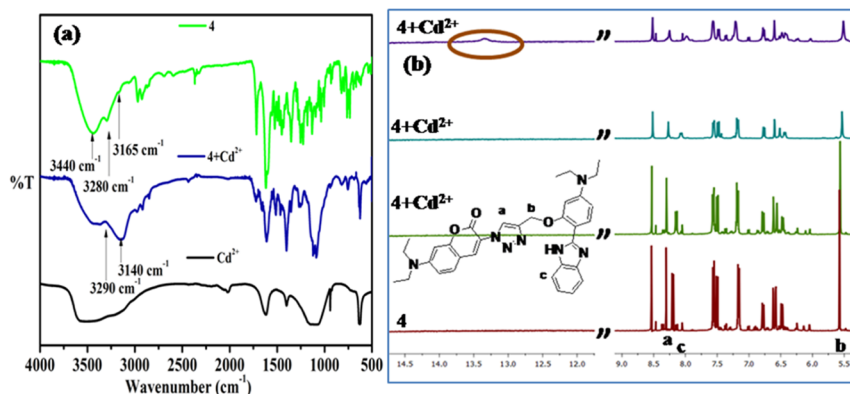

Figure 4. (a) FTIR spectra of **4**, **4:Cd²⁺**, and Cd(ClO₄)₂ and (b) ¹H NMR titration spectra of **4** with Cd²⁺ in d_3-ACN.
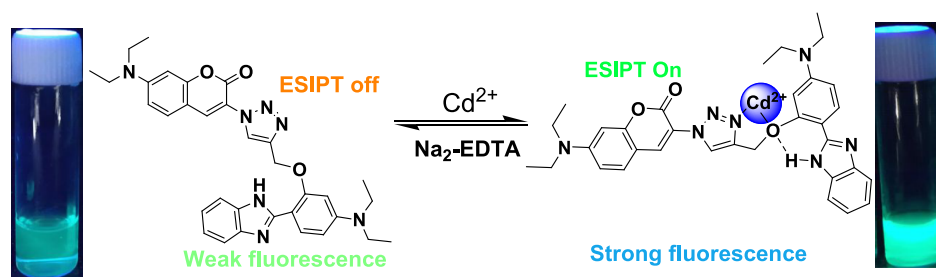
Figure 5. Proposed mode of binding of **4** toward Cd²⁺.
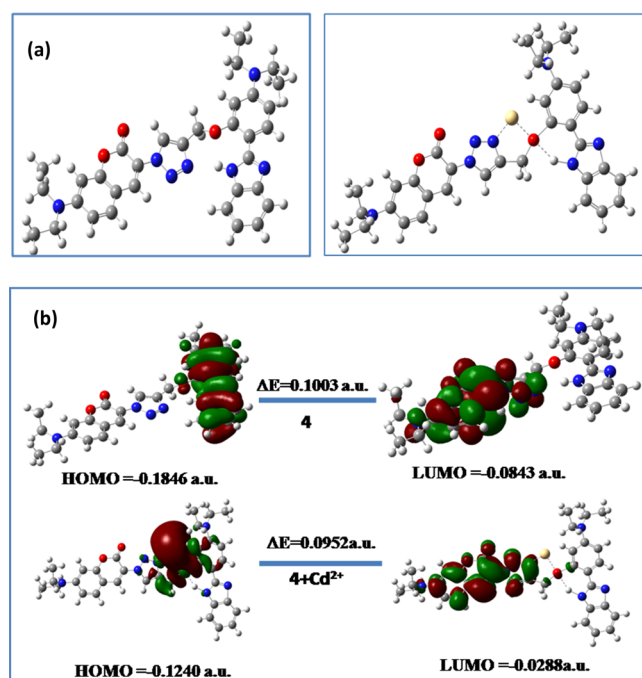
Figure 6. (a) Energy-optimized structures of **4** and **4:Cd²⁺** and (b) HOMO−LUMO energy level diagram of **4** and **4:Cd²⁺**.

2.8. Biological Application: A Cell Imaging Study. The C6 (rat glial cell) and HEP G2 (human liver cell) cell lines were used for the cell viability test. For the cytotoxicity test, **4** was incubated into the cells for 2 h. Methyl thiazolyl tetrazolium (MTT) assay was used to measure the cell viability of the sensor, whereas LDA assay was used for the cytotoxicity test. Then, Cd²⁺ salt was added in phosphate-buffered saline (PBS) to the pre-treated cells for 15 min to check the sensing, and the excess metal ion was removed accordingly. The images were taken by using a Leica DMi8 fluorescence microscope.

2.9. Cell Viability and Cytotoxicity Test. To measure the effect of **4** on living cells, cell viability and cytotoxicity test were carried out in two cell lines, C6 (rat glial cell) and Hep G2 (human liver cell), using PBS MTT assay. As shown in Figure 8a, the cell viability for both the cells was reached up to a concentration of 50 μM. Furthermore, the cytotoxicity of the sensor was checked, and the corresponding results are shown in Figure 8. The experimental results confirmed that the sensor (**4**) remained noncytotoxic up to the concentration of 50 μM.

For the real-time application of sensor **4**, cell imaging analysis was performed using two cell lines, C6 (rat glial cell) and Hep G2 (human liver cell). However, upon treatment with **4**, a very weak fluorescence was observed with C6 (rat glial cell), as shown in Figure 9 (i). The cells were incubated with different concentrations of Cd²⁺ for 2 h. Sensor **4** was added to the cells with a concentration of 10 μM and left for another 15 min. After that, the cells were used for further treatment, and images were taken as shown in profile A in Figure 9. Panel B represented the measurement of the line profile of the fluorescent intensity of **4** after binding with Cd²⁺. Both the cells exhibited the same results (Figure 10), and the experiments confirmed that **4** might be a suitable reagent for the detection of Cd²⁺ in live cells.

2.10. Single-Crystal X-ray Analysis. Sensor **4** has been synthesized using an easy synthetic procedure, as shown in Scheme 1. The structure of sensor **4**, and all the compounds, was confirmed by ¹H and ¹³C NMR, ESI mass spectra, and FTIR analysis. Fortunately, we got a single crystal of compound **3** (CCDC no. 1995732), the precursor of the final step. The yellow-colored crystal was grown through the solvent evaporation technique from ethyl acetate solvent. Compound **3** had a monoclinic crystal system with a $P121/c1$ space group. As shown in Figure 11, the entire molecule was planar and the aldehyde group was placed opposite to the triazole moiety, which was further used for benzimidazole formation. The details of the experimental data are given in Supporting Information.

3. EXPERIMENTAL SECTION

3.1. General. All the required reagents and chemicals for this work were purchased from Merck and used without further purification. The HPLC-UV-grade CH₃CN was used in all spectroscopic measurements. NMR analysis was carried out on a Brucker 400 MHz instrument using CDCl₃, DMSO-d_6, and d₃-CH₃CN. HRMS and ESI−MS measurements were carried out on XEVO G2-XS QTOF. FTIR spectra were recorded on a spectrum 2000 PerkinElmer spectrometer. UV−vis and emission spectra were recorded on a Lambda 635PerkimElmer spectrophotometer and a LS-55 PerkinElmer spectrophotometer, respectively. FESEM analysis was carried out on a Supra 55 Carl Zeiss Germany instrument. The single-crystal XRD data were recorded on SuperNovaG8910B. A Remco hot stage melting point apparatus was used for measuring the melting point.

3.2. FESEM Analysis. FESEM images were recorded using Supra 55 (Carl Zeiss). Samples for FESEM were prepared by slow evaporation of the sensor and complex, which were drop-casted on a 1.0×1.0 cm² glass plate and dried overnight in the air inside a desiccator. The samples were then sputter-coated with Au and subjected to a FESEM study.

3.3. Cell Viability Assay. MTT assay was used to measure the cytotoxic potential of SM227. Rat glial cells (C6) and human liver cells (HepG2) were seeded in a 96-well cell-culture plate. Various concentrations (1, 10 μM, 1, and 10 nM)
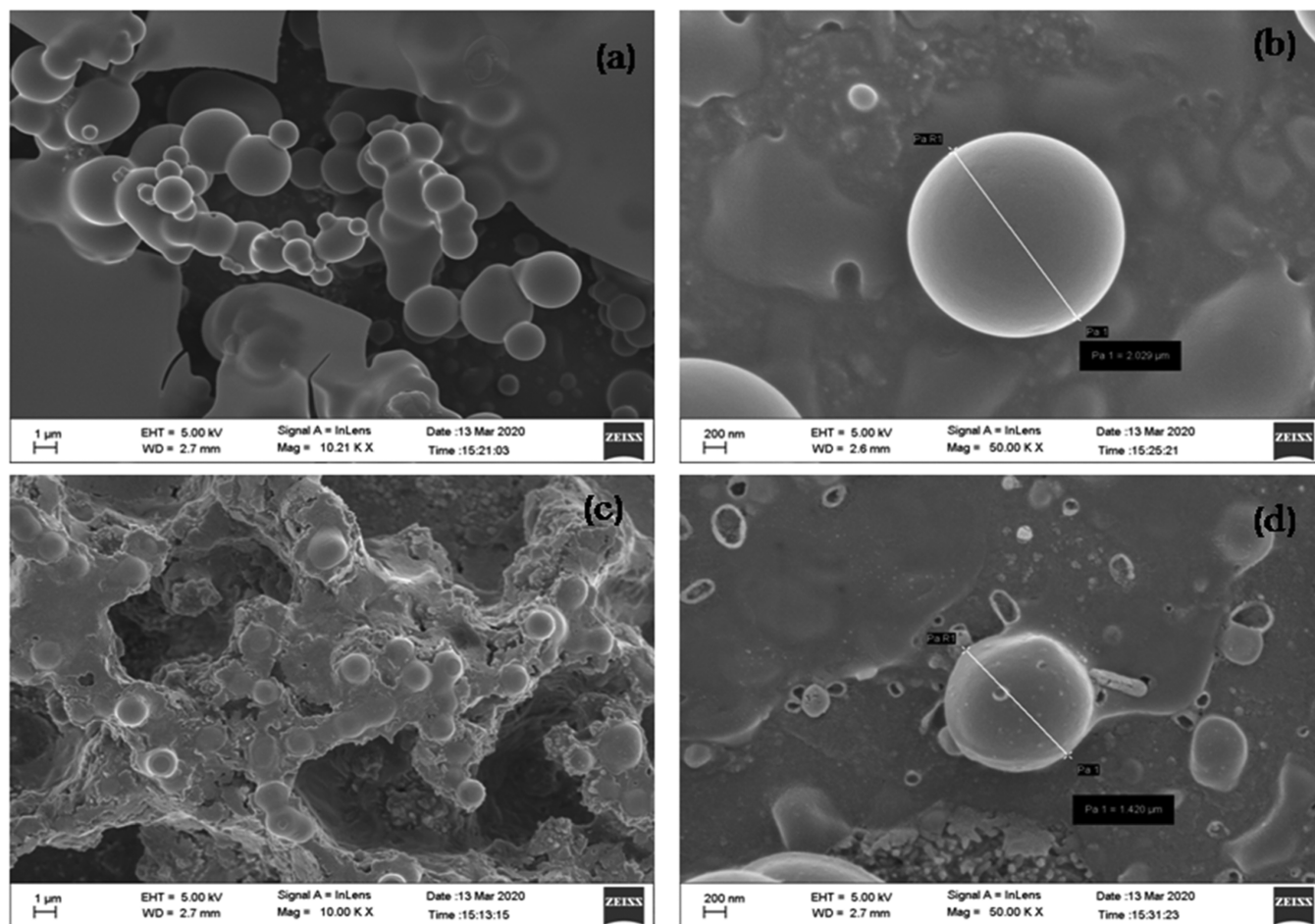
Figure 7. FESEM images of (a,b) **4** with regular diameter and (c,d) **4:Cd^{2+}** with deformed diameter.
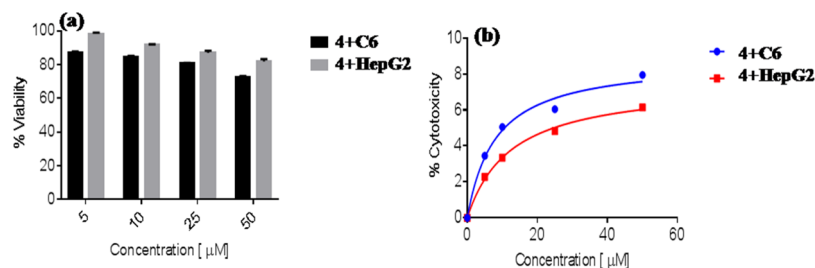

Figure 8. (a) Cell viability and (b) cytotoxicity test of **4** in C6 and Hep G2 cell lines.

of **4** were added to the cells. The cells were incubated at 37 °C under 5% CO$_2$ for 24 h. 10 μL of MTT (5 mg mL^{-1}) was added to each well and incubated at 37 °C under 5% CO$_2$ for 4 h. The MTT solution was removed, and yellow precipitates (formazan) observed in plates were dissolved in 200 μL of acidic isopropanol. Multiskan GO microplate spectrophotometer was used to measure the absorbance at 570 nm for each well. The viability of cells was calculated according to the following equation

$$\% \text{ Cell viability} = \left[\frac{\text{experimental OD570}}{\text{control OD570}} \right] \times 100$$

3.4. Synthesis of 4-(Diethylamino)-2-(prop-2-ynyloxy)benzaldehyde (1). A mixture of 4-(diethylamino)-salicylaldehyde and K$_2$CO$_3$ was refluxed in acetone for 30 min. After that, 1 equivalent of propargyl bromide was added, and

the mixture was refluxed for another 4 h. The crude product was extracted with ethyl acetate and purified by flash column chromatography using ethyl acetate and petroleum ether as the eluent (3:7). Compound **1** was isolated as a yellow-coloured liquid.

3.4.1. ^{1}H NMR of Compound 1 (400 MHz, CDCl$_3$). ^{1}H NMR of compound **1** (400 MHz, CDCl$_3$): δ 9.96 (s, 1H), 7.51 (d, 1H, J = 8.0 Hz), 6.12 (d, 1H, J = 8.0 Hz), 6.05 (s, 1H), 4.63 (s, 2H), 3.24 (t, 4H, J = 4.0 Hz), 2.57 (s, 1H), 1.03 (t, 6H, J = 4.0 Hz); ^{13}C NMR (100 MHz, CDCl$_3$): 186.2, 161.9, 153.5, 130.1, 114.1, 104.8, 94.0, 76.4, 55.8, 44.7, 12.4.

3.5. Preparation of 3-Azido-7-(diethylamino)-2H-chromen-2-one (2).[33] A mixture containing *n*-butanol (20.0 mL), 4-diethylaminosalicylaldehyde (1.4 g and 7.2 mmol), ethylnitroacetate (0.8 mL and 7.2 mmol), molecular sieves 4 Å (100 mg), piperidine (0.1 mL), and acetic acid (0.2
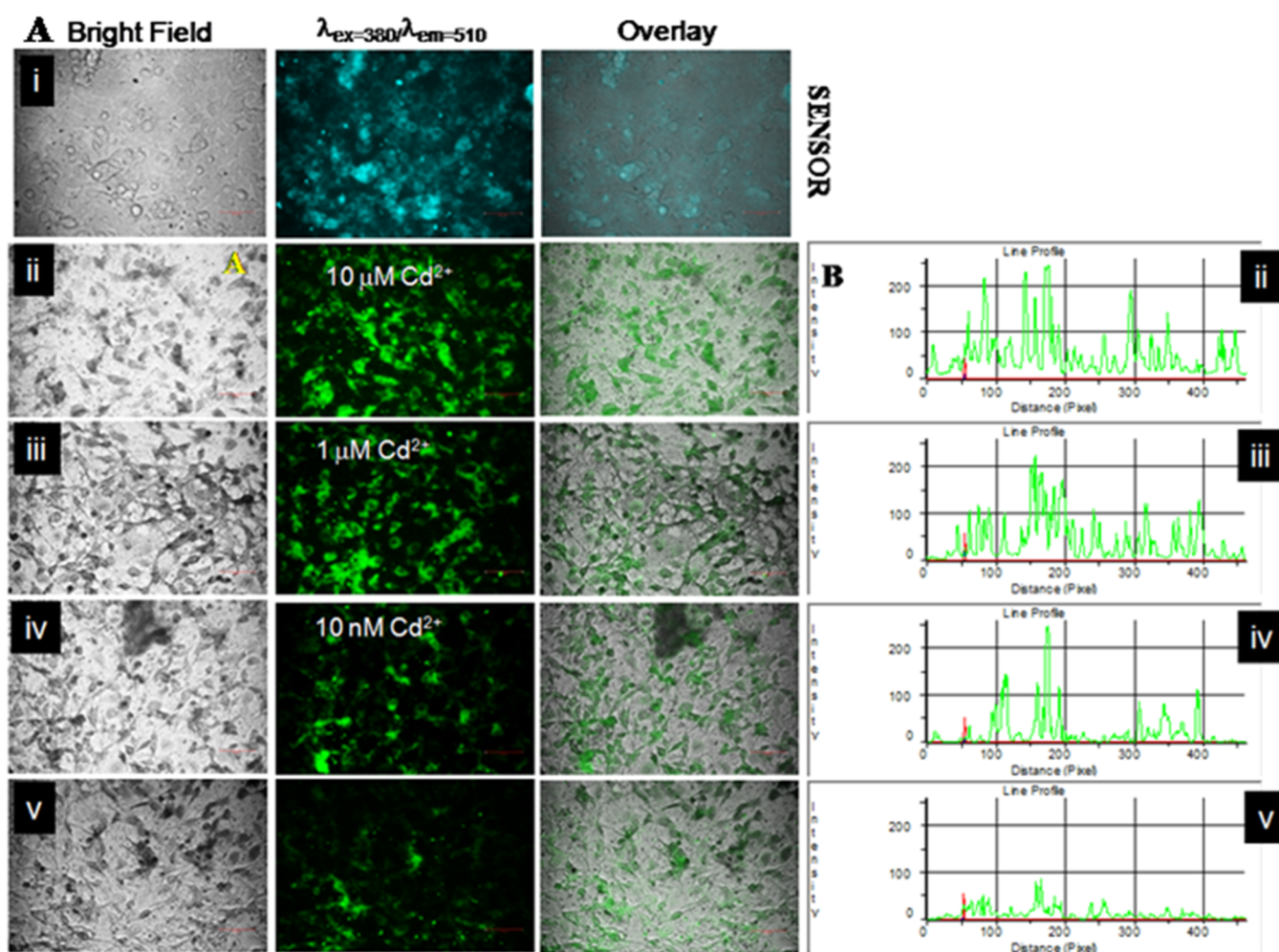
Figure 9. Fluorescence images of C6 (rat glial cell) with **4** (8.66 μM) in the presence of Cd²⁺ (panel A) and line profile of fluorescent intensity of **4** with different concentrations of Cd²⁺ (panel B).

mL) was refluxed for a period of 24 h. Upon cooling to room temperature, a bright yellow solid was formed, which was collected and dissolved in dimethylformamide (15 mL) at 80 °C. It was filtered again to remove the molecular sieves. The filtrate, upon addition to 100 mL of ice-cold water, yielded 3-nitro-7-diethylaminocoumarin as a bright yellow solid (1.40 g and 73%).

3-Nitro-7-diethylaminocoumarin (0.25 g and 0.95 mmol) was added consequently to a suspension of stannous chloride dihydrate (1.6 g and 7.12 mmol) in HCl in a round-bottom flask placed on a magnetic stirrer to stir for 4 h. The solid product was obtained through neutralization of the suspension using aqueous sodium hydroxide. In this way, 7-diethylamino-3-aminocoumarin was prepared and ready to use further for the next step. 7-Diethylamino-3-aminocoumarin (100 mg and 0.43 mmol) was dissolved slowly in HCl aq (17.2% and 4 mL) at room temperature. Upon cooling to 0−5 °C and the addition of a solution of NaNO₂ (30 mg and 0.43 mmol), the reaction mixture was stirred for 1 h. Then, potassium acetate (2.0 g) was added to the water (5 mL) to adjust pH 4. Sodium azide (57 mg and 0.88 mmol) was added in portions to the mixture and stirred at 0−5 °C for another 5 h. The precipitate was rapidly filtered and washed with ice-cold water. Finally, the product was dried under a vacuum to yield the pure material, 3-azido-7-(diethylamino)-2H-chromen-2-one (**2**), as a yellow solid.

3.6. Synthesis of Compound 3. Compound **1** (0.55 g and 2.38 mmol) was dissolved in an ethanol/H₂O (1:1) mixture and stirred for half an hour. After that, coumarin azide (0.61 g and 2.38 mmol), sodium ascorbate, and copper sulfate were added to this solution. The resulting mixture was allowed to stir overnight at room temperature. Upon completion of the reaction, the mixture was filtered and evaporated out of the solvent. Then, water was added to it and further extracted with ethyl acetate. The organic layer was dried under a vacuum, and the desired product (**3**) was obtained via column chromatography using ethyl acetate/petroleum ether (3:7) as the eluent. Yield: 68% (0.79 g).

3.6.1. ¹H NMR (400 MHz, CDCl₃). ¹H NMR (400 MHz, CDCl₃): δ10.07 (s, 1H), 8.58 (s, 1H), 8.28 (s, 1H), 7.62 (d, 1H, J = 8.8 Hz), 7.31 (d, 1H, J = 8.8 Hz), 6.57 (d, 1H, J = 4.0 Hz), 6.46 (s, 1H), 6.25 (s, 1H), 6.21 (d, 1H, J = 8.8 Hz), 5.30 (s, 2H), 3.35 (q, 8H, J = 4.4 Hz), 1.14 (t, 12H, J = 4.4 Hz). ¹³C NMR (100 MHz, CDCl₃): 186.9, 162.9, 256.9, 155.8, 153.7, 151.6, 143.4, 134.9, 130.5, 130.0, 126.0, 116.6, 114.3, 110.1, 106.9, 104.7, 97.0, 94.0, 62.15, 45.0, 44.0, 12.6, 12.4. FTIR data (KBr, cm⁻¹): 2990, 1720, 1605, 1590, 1433, 1400. ESI-HRMS (+ve mode, m/z): calcd 489.23; found, 490.23 (M + H)⁺. mp: 94−96 °C.

3.7. Synthesis of Compound 4. To a solution of **3** (20.0 mg and 0.041 mmol) in dry methanol (5.0 mL), o-phenylenediamine (5.20 mg and 0.0416 mmol) and sodium
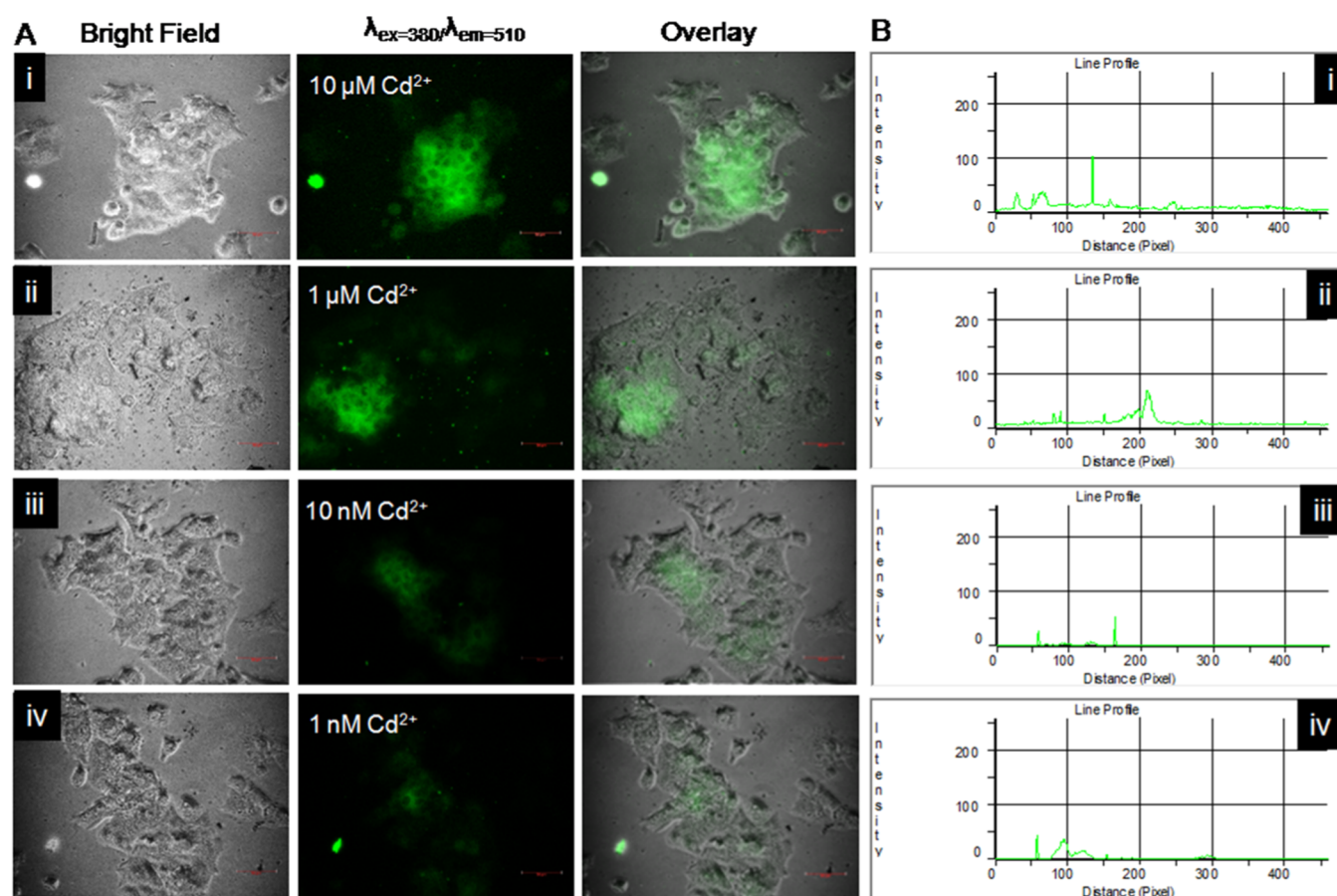
Figure 10. Fluorescence images of Hep G2 (human liver cell) with **4** (8.66 μM) in the presence of Cd^{2+} (panel A) and line profile of fluorescent intensity of **4** with different concentrations of Cd^{2+} (panel B).
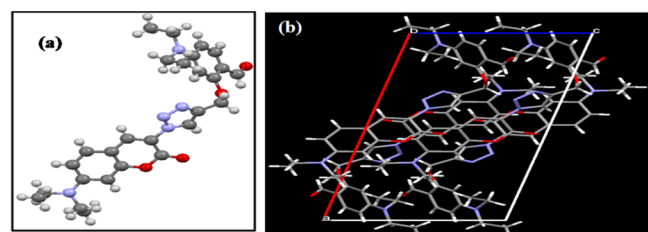

Figure 11. Single crystal X-ray (a) ORTEP structure of **3** and (b) its packing structure.

bisulfate (5.0 mg and 0.0416 mmol) were added. The mixture was refluxed for 5 h in an N$_2$ atmosphere. The crude product was extracted with ethyl acetate and washed with distilled water. The organic layer was dried over anhydrous sodium sulfate and purified by silica gel column chromatography using ethyl acetate/petroleum ether (2:8) to afford **4** (yield 55%).

3.7.1. ^{1}H NMR (400 MHz, CDCl$_3$). ^{1}H NMR (400 MHz, CDCl$_3$): δ 8.52 (s, 1H), 8.29 (s, 1H), 8.17 (d, J = 8.0 Hz 1H), 7.55−7.53 (m, 2H), 7.16−7.14 (m, 2H), 6.77 (dd, J = 8.0, Hz, 1H), 6.60 (s, 1H), 6.56 (s, 1H), 6.46 (dd, J = 8.0 Hz, 1H), 5.56 (s, 2H), 3.44 (q, J = 4.0 Hz, 8H), 1.19 (t, J = 4.0 Hz, 6H), 1.16 (t, J = 4.0 Hz, 6H); ^{13}C NMR (100 MHz, CDCl$_3$): 157.5, 156.9, 155.9, 151.8, 150.6, 150.4, 143.1, 135.1, 131.4, 130.1, 122.8, 121.8, 116.5, 110.2, 106.9, 106.0, 97.0, 95.8, 62.8, 45.8, 12.6; HRMS (ESI +ve mode, m/z): calc 577.2801; found, 578.2874 [M + H]. FTIR data (KBr, cm^{-1}): 3440, 3280, 1719, 1605, 1530, 1433, 1400. mp: 104−106 °C.

4. CONCLUSIONS

In summary, a new and simple triazole-bridged coumarin−benzimidazole-conjugated fluorescent sensor **4** was developed for selective detection of Cd^{2+}, and an ESIPT-based turn-on fluorescence response has been observed during complexation. The mechanism of interaction was explicated with the help of ^{1}H NMR, ESI mass, and FTIR analysis. Furthermore, sensor **4** was applied to the living cells for a bio-imaging study in order to get a real-time application. The single-crystal X-ray analysis confirmed the geometry of **3** for encapsulating the metal ion..

■ ASSOCIATED CONTENT

ⓢ Supporting Information

The Supporting Information is available free of charge at https://pubs.acs.org/doi/10.1021/acsomega.1c03793.

> Analytical data of the synthesized compounds, visual color change of **4**, reversibility of sensor **4**, ESI mass spectra, crystal structures, methods of theoretical calculation and the crystallographic data, and comparison table of the recently published Cd^{2+} sensor (PDF)
> Shelxl refinement (CIF)

■ AUTHOR INFORMATION

Corresponding Author

Swapan Dey − *Department of Chemistry, Indian Institute of Technology (ISM), Dhanbad 826004, India;* ⓘ orcid.org/0000-0002-6168-5627; Phone: +91 326 2235607; Email: swapan@iitism.ac.in; Fax: +91 326 2296563

Author

Surajit Mondal − *Department of Chemistry, Indian Institute of Technology (ISM), Dhanbad 826004, India*

Complete contact information is available at:
https://pubs.acs.org/10.1021/acsomega.1c03793

Notes

The authors declare no competing financial interest.

■ REFERENCES

(1) Zhou, S.-F.; Wang, J.-J.; Gan, L.; Han, X.-J.; Fan, H.-L.; Mei, L.-Y.; Huang, J.; Liu, Y.-Q. Individual and simultaneous electrochemical detection toward heavy metal ions based on L-cysteine modified mesoporous MnFe2O4 nanocrystal clusters. *J. Alloys Compd.* **2017**, *721*, 492−500.

(2) Guo, S.; Liu, G.; Fan, C.; Pu, S. A highly selective fluorescent probe for detection of Cd2+ and HSO3− based on photochromic diarylethene with a triazole-bridged coumarin-quinoline group. *RSC Adv.* **2018**, *8*, 22786−22798.

(3) Quang, D. T.; Kim, J. S. Fluoro- and Chromogenic Chemodosimeters for Heavy Metal Ion Detection in Solution and Biospecimens. *Chem. Rev.* **2010**, *110*, 6280−6301.

(4) Hao, J.-N.; Yan, B. A water-stable lanthanide-functionalized MOF as a highly selective and sensitive fluorescent probe for Cd2+. *Chem. Commun.* **2015**, *51*, 7737−7740.

(5) Lv, Y.; Wu, L.; Shen, W.; Wang, J.; Xuan, G.; Sun, X. A porphyrin-based chemosensor for colorimetric and fluorometric detection of cadmium(II) with high selectivity. *J. Porphyr. Phthalocyanines* **2015**, *19*, 769−774.

(6) Klaassen, C. D.; Liu, J.; Diwan, B. A. Metallothionein protection of cadmium toxicity. *Toxicol. Appl. Pharmacol.* **2009**, *238*, 215−220.

(7) Xu, X.-Y.; Yan, B. Eu(III) functionalized Zr-based metal-organic framework as excellent fluorescent probe for Cd2+ detection in aqueous environment. *Sens. Actuators, B* **2016**, *222*, 347−353.

(8) Luo, Y.; Tang, D.; Zhu, W.; Xu, Y.; Qian, X. Reactive fluorescent dye functionalized cotton fabric as a "Magic Cloth" for selective sensing and reversible separation of Cd2+ in water. *J. Mater. Chem.* **2015**, *3*, 8485−8489.

(9) Mehta, V. N.; Rohit, J. V.; Kailasa, S. K. Functionalization of silver nanoparticles with 5-sulfoanthranilic acid dithiocarbamate for selective colorimetric detection of Mn2+ and Cd2+ ions. *New J. Chem.* **2016**, *40*, 4566−4574.

(10) Mohanasundaram, D.; Bhaskar, R.; Kumar, G. G. V.; Rajesh, J.; Rajagopal, G. A quinoline based Schiff base as a turn-on fluorescence chemosensor for selective and robust detection of Cd2+ ion in semi-aqueous medium. *Microchem. J.* **2021**, *164*, 106030.

(11) Gasparik, J.; Vladarova, D.; Capcarova, M.; Smehyl, P.; Slamecka, J.; Garaj, P.; Stawarz, R.; Massanyi, P. Concentration of lead, cadmium, mercury and arsenic in leg skeletal muscles of three species of wild birds. *J. Environ. Sci. Health, Part A: Toxic/Hazard. Subst. Environ. Eng.* **2010**, *45*, 818−823.

(12) Caroli, S.; Forte, G.; Iamiceli, A.; Galoppi, B. Determination of essential and potentially toxic trace elements in honey by inductively coupled plasma-based techniques. *Talanta* **1999**, *50*, 327−336.

(13) Townsend, A. T.; Miller, K. A.; McLean, S.; Aldous, S. The determination of copper, zinc, cadmium and lead in urine by high resolution ICP-MS. *J. Anal. At. Spectrom.* **1998**, *13*, 1213−1219.

(14) Bharti, A.; Ma, P. C.; Salgia, R. Biomarker discovery in lung cancer-promises and challenges of clinical proteomics. *Mass Spectrom. Rev.* **2007**, *26*, 451−466.

(15) Mimendia, A.; Legin, A.; Merkoçi, A.; del Valle, M. Use of Sequential Injection Analysis to construct a potentiometric electronic tongue: Application to the multideterminations of heavy metals. *Sens. Actuators, B* **2010**, *146*, 420−426.

(16) Liu, Z.; He, W.; Guo, Z. Metal coordination in photo-luminescent sensing. *Chem. Soc. Rev.* **2013**, *42*, 1568−1600.

(17) Ko, S.-K.; Chen, X.; Yoon, J.; Shin, I. Zebrafish as a good vertebrate model for molecular imaging using fluorescent probes. *Chem. Soc. Rev.* **2011**, *40*, 2120−2130.

(18) Zhang, J. F.; Zhou, Y.; Yoon, J.; Kim, J. S. Recent progress in fluorescent and colorimetric chemosensors for detection of precious metal ions (silver, gold and platinum ions). *Chem. Soc. Rev.* **2011**, *40*, 3416−3429.

(19) Wang, Q.; Xie, Y.; Ding, Y.; Li, X.; Zhu, W. Colorimetric fluoride sensors based on deprotonation of pyrrole-hemiquinone compounds. *Chem. Commun.* **2010**, *46*, 3669−3671.

(20) Dhanushkodi, M.; Vinoth Kumar, G. G.; Balachandar, B. K.; Sarveswari, S.; Gandhi, S.; Rajesh, J. A simple pyrazine based ratiometric fluorescent sensor for Ni2+ ion detection. *Dyes Pigm.* **2020**, *173*, 107897.

(21) Mohanasundaram, D.; Vinoth Kumar, G. G.; Kumar, S. K.; Maddiboyina, B.; Raja, R. P.; Rajesh, J.; Sivaraman, G. Turn-on fluorescence sensor for selective detection of fluoride ion and its molecular logic gates behavior. *J. Mol. Liq.* **2020**, *317*, 113913.

(22) Cardoso, M. B.; Samios, D.; da Silveira, N. P.; Rodembusch, F. S.; Stefani, V. ESIPT-exhibiting protein probes: a sensitive method for rice proteins detection during starchextraction. *Photochem. Photobiol. Sci.* **2007**, *6*, 99−102.

(23) Goswami, S.; Manna, A.; Paul, S.; Das, A. K.; Aich, K.; Nandi, P. K. Resonance-assisted hydrogen bonding induced nucleophilic addition to hamper ESIPT: ratiometric detection of cyanide in aqueous media. *Chem. Commun.* **2013**, *49*, 2912−2914.

(24) Sedgwick, A. C.; Wu, L.; Han, H.-H.; Bull, S. D.; He, X.-P.; James, T. D.; Sessler, J. L.; Tang, B. Z.; Tian, H.; Yoon, J. Excited-state intramolecular proton-transfer (ESIPT) based fluorescence sensors and imaging agents. *Chem. Soc. Rev.* **2018**, *47*, 8842−8880.

(25) Helal, A.; Thao, N. T. T.; Lee, S. W.; Kim, H.-S. Thiazole-based chemosensor II: synthesis and fluorescence sensing of fluoride ions based on inhibition of ESIPT. *J. Inclusion Phenom. Macrocyclic Chem.* **2010**, *66*, 87−94.

(26) Kenchappa, R.; Bodke, Y. D.; Telkar, S.; Aruna Sindhe, M. Antifungal and anthelmintic activity of novel benzofuran derivatives containing thiazolo benzimidazole nucleus: an in vitro evaluation. *J. Chem. Biol.* **2017**, *10*, 11−23.

(27) Jung, H. S.; Han, J. H.; Kim, Z. H.; Kang, C.; Kim, J. S. Coumarin-Cu(II) Ensemble-Based Cyanide Sensing Chemodosimeter. *Org. Lett.* **2011**, *13*, 5056−5059.

(28) Song, H.; Zhang, Z. A quinoline-based ratiometric fluorescent probe for discriminative detection of Zn2+ and Cd2+ with different binding modes, and its Zn2+ complex for relay sensing of pyrophosphate and adenosine triphosphate. *Dyes Pigm.* **2019**, *165*, 172−181.

(29) Areti, S.; Bandaru, S.; Rao, C. P. Triazole-linked quinoline conjugate of glucopyranose: selectivity comparison among Zn2+, Cd2+, and Hg2+ based on spectroscopy, thermodynamics, and microscopy, and reversible sensing of Zn2+ and the structure of the complex using DFT. *ACS Omega* **2016**, *1*, 626−635.

(30) Kumari, C.; Sain, D.; Kumar, A.; Debnath, S.; Saha, P.; Dey, S. Intracellular detection of hazardous Cd2+ through a fluorescence imaging technique by using a nontoxic coumarin based sensor. *Dalton Trans.* **2017**, *46*, 2524−2531.

(31) Kumari, C.; Sain, D.; Kumar, A.; Debnath, S.; Saha, P.; Dey, S. A real time colorimetric 'two in one' kit for tracking ppb levels of uric acid and Hg2+ in live HeLa S3 cells and Hg2+ induced keto-enol tautomerism. *RSC Adv.* **2016**, *6*, 62990−62998.

(32) Kumar, A.; Mondal, S.; Kayshap, K. S.; Hira, S. K.; Manna, P. P.; Dehaen, W.; Dey, S. Water switched aggregation/disaggregation strategies of a coumarin-naphthalene conjugated sensor and its selectivity towards Cu2+ and Ag+ ions along with cell imaging studies on human osteosarcoma cells (U-2 OS). *New J. Chem.* **2018**, *42*, 10983−10988.

(33) Sivakumar, K.; Xie, F.; Cash, B. M.; Long, S.; Barnhill, H. N.; Wang, Q. A Fluorogenic 1,3-Dipolar Cycloaddition Reaction of 3-Azidocoumarins and Acetylenes†. *Org. Lett.* **2004**, *6*, 4603−4606.

(34) Shortreed, M.; Kopelman, R.; Kuhn, M.; Hoyland, B. Fluorescent fiber-optic calcium sensor for physiological measurements. *Anal. Chem.* **1996**, *68*, 1414−1418.

(35) Yang, Y.; Cheng, T.; Zhu, W.; Xu, Y.; Qian, X. Highly selective and sensitive near-infrared fluorescent sensors for cadmium in aqueous solution. *Org. Lett.* **2011**, *13*, 264−267.

(36) Benesi, H. A.; Hildebrand, J. H. A spectrophotometric investigation of the interaction of iodine with aromatic hydrocarbons. *J. Am. Chem. Soc.* **1949**, *71*, 2703−2707.

(37) Chou, P.-T.; Wu, G.-R.; Wei, C.-Y.; Cheng, C.-C.; Chang, C.-P.; Hung, F.-T. Excited-State Amine−Imine Double Proton Transfer in 7-Azaindoline. *J. Phys. Chem. B* **2000**, *104*, 7818−7829.

(38) Barman, S.; Mukhopadhyay, S. K.; Gangopadhyay, M.; Biswas, S.; Dey, S.; Singh, N. D. P. Coumarin-benzothiazole-chlorambucil (Cou-Benz-Cbl) conjugate: an ESIPT based pH sensitive photo-responsive drug delivery system. *J. Mater. Chem. B.* **2015**, *3*, 3490−3497.

(39) Chen, W.-H.; Xing, Y.; Pang, Y. A highly selective pyrophosphate sensor based on ESIPT turn-on in water. *Org. Lett.* **2011**, *13*, 1362−1365.

(40) Jayabharathi, J.; Thanikachalam, V.; Jayamoorthy, K. Synthesis of some fluorescent benzimidazole derivatives using cobalt(ii) hydroxide as highly efficient catalyst - spectral and physico-chemical studies and ESIPT process. *Photochem. Photobiol. Sci.* **2013**, *12*, 1761−1773.

(41) Sinha, S.; Chowdhury, B.; Ghosh, P. A highly sensitive ESIPT-based ratiometric fluorescence sensor for selective detection of Al3+. *Inorg. Chem.* **2016**, *55*, 9212−9220.

(42) Schulman, S. G. *Molecular Luminescence Spectroscopy*; Wiley, 1985.

(43) Cheng, D.; Liu, X.; Xie, Y.; Lv, H.; Wang, Z.; Yang, H.; Han, A.; Yang, X.; Zang, L. A ratiometric fluorescent sensor for Cd2+ based on internal charge transfer. *Sensors* **2017**, *17*, 2517.

(44) Crowley, J. D.; McMorran, D. A. "Click-Triazole" Coordination Chemistry: Exploiting 1,4-Disubstituted-1,2,3-Triazoles as Ligands. *Click Triazoles*; Springer, 2012; pp 31−83.

(45) Frisch, M.; Trucks, G.; Schlegel, H.; Scuseria, G.; Robb, M.; Cheeseman, J.; Scalmani, G.; Barone, V.; Mennucci, B.; Petersson, G. *Gaussian09*, Revision D. 01; Gaussian Inc: Wallingford CT, 2009. See also: URL: http://www.gaussian.com.

(46) Dennington, R.; Keith, T. A.; Millam, J. M. *GaussView 5.0*; Gaussian. Inc.: Wallingford, 2008.

(47) Bourbon, P.; Peng, Q.; Ferraudi, G.; Stauffacher, C.; Wiest, O.; Helquist, P. Synthesis, photophysical, photochemical, and computational studies of coumarin-labeled nicotinamide derivatives. *J. Org. Chem.* **2012**, *77*, 2756−2762.

(48) Fegade, U.; Sahoo, S. K.; Singh, A.; Mahulikar, P.; Attarde, S.; Singh, N.; Kuwar, A. A selective and discriminating noncyclic receptor for HSO4− ion recognition. *RSC Adv.* **2014**, *4*, 15288−15292.

(49) Wu, Y.; Wen, X.; Fan, Z. An AIE active pyrene based fluorescent probe for selective sensing Hg2+ and imaging in live cells. *Spectrochim. Acta, Part A* **2019**, *223*, 117315.